Prediction and Interpretation of Combustion Processes in Natural Gas Engines – A comparative Overview of Simulation Methods for Practical Applications

Christian Lämmle[1),2)], Konstantinos Boulouchos[1)], Christian Bach[2)]

1) Aerothermochemistry and Combustion Systems Laboratory (LAV), ETH Zürich, CH-Zürich
2) Swiss Federal Laboratories for Materials Testing and Research, EMPA, CH-Dübendorf

Abstract

One of the major objectives during the development process is to reduce costs and time to market. Increasing computational power and continuous improvements of models for internal combustion engine applications promise to replace some optimisation steps by computer simulations. A prerequisite for that is that trends can be reasonably predicted and that calculations adequately incorporate the physics to support the understanding of the complex processes involved.

Different simulation tools are used depending on the objectives of a specific calculation. These tools can be distinguished by the complexity of the models, where the model depth, the information content and the computational time demand vary significant.

In this paper three types of combustion models are presented. An empirical model was developed based on experimentally determined burn rates to predict engine behaviour for a wide range of operating conditions. Extensive parameter variations have been investigated. The compression ratio was optimised and an accurate turbocharger was found to meet the objectives.

The phenomenological model can be used to predict engine behaviour and to additionally support the understanding of the experimental results. The burning behaviour for two combustion chamber designs was explained by analysing the flame front area.

3-Dimensional calculations were used to support the findings for some single engine operating points and allowed to visualise local effects.

During a collaborative project (CEV) for developing an ultra-low-emission vehicle gas engine [4] among other measures the compression ratio was increased to reduce fuel consumption and to utilise the favourable thermo-chemical properties of compressed natural gas. This modification influences on one hand the thermodynamic process and on the other hand the combustion chamber geometry and therefore the flame propagation. The different simulation tools will be discussed and compared in the frame of this specific application.

1. Introduction

One of the major challenges for the next few years will be to reduce CO_2-emissions in the mobility sector. Agreements have been made between public authorities and car manufacturers [3] and importers [1].

The CNG (Compressed Natural Gas) vehicle has a high potential for improvement of air quality and for significant reductions in CO_2-Emissions. The fuel scenario of the European Commission until 2020 [2] includes the promotion of natural gas for transportation. Furthermore compressed natural gas will help to reduce the dependence on crude oil.

During the CEV (Clean Engine vehicle)-project modifications on a gasoline fuelled engine were carried out and contributed to a reduction of CO_2-emissions about 30% in monovalent CNG operation compared to a gasoline production car with equivalent performance. Furthermore, the CEV fulfils the European EURO 4 and the Californian Super-Ultra-Low-Emission-Vehicles (SULEV) emission standards. The engine was operated with λ=1 in the whole map. New catalyst converters dedicated to CNG operation have been applied.

This project was a collaboration among the EMPA Dübendorf and the ETH Zürich. VW Wolfsburg, Bosch, Corning and Engelhard were the industrial partners. The project was funded by the Swiss Federal Office of Energy, the Swiss Gas and Water Industry Association SVGW, the German technical and scientific organization on Gas and water DVGW and by the Austrian Gas and Water Industry Association ÖVGW.

The overall strategy of the CEV focused on increasing the part load efficiency. The compression ratio was increased to reduce fuel consumption, thus the compression ratio had to be optimised. Due to the power loss in CNG operation at full load an adequate turbocharger was installed. The high octane number of compressed natural gas allowed driving the engine with high compression ratio and turbocharger. Further reductions in CO_2-Emission could be achieved by changing the transmission and optimising the EGR distribution in the intake manifold whereon the EGR-Rate was increased. All these modifications offer a lot of possible driving strategies. Simulation tools have been utilised successfully to find the optimal strategy.

2. Applied simulation tools

For the backward calculation – that means the calculation of the burn rate based on measured cylinder pressure data - the LAV code WEG was used. For the forward calculation GT-Power was used where the empirical and the phenomenological models integrated by user subroutines replaced the standard combustion models. All these codes use a two zone model for the thermodynamic in-cylinder process. The 3D code applied was StarCD.

3. Project engine

All the tests were performed on a 4 cylinder 1-liter engine with two valves per cylinder. The compression ratio of the production engine is ε=10.7 and it is equipped with an EGR system without cooling. Bore and stroke are 67.1mm and 70.6mm, respectively.

4. Combustion basics

For the empirical model, a Vibe curve was used to approximate the burn rate, whereas global approaches for the flame speed, the in-cylinder turbulence and the flame front area have been introduced for the phenomenological case. The standard models of StarCD were used for the 3D calculations.

4.1. Empirical combustion model

The empirical combustion model is based on the conversion of the Vibe parameters depending on the engine operating conditions. Starting from a fixed engine operating point one parameter is changed while the others are kept constant. By analysing the burn rate from measured cylinder pressure curves and adjusting the Vibe parameters to match these experimental data, rules can be defined how the burn rate has to be changed for each of the investigated engine parameter. The resulting conversion factors for the Vibe parameters are obtained by superposing the individual effects.

Existing “Vibe parameter conversion”-models have been developed for gasoline engines [5], [9] or for lean burn natural gas engines [10] and have been tested successfully. A fast and simple empirical combustion model for stoichiometric natural gas engines for automotive applications is missing.

The burn rate is defined by the total amount of fuel mass m_F, a rate of change of a combustion progress variable x_B and the lower heating value H_L:

$$\frac{\partial Q_B}{\partial \varphi} = \frac{\partial m_F}{\partial \varphi} \cdot H_L = m_F \cdot \frac{\partial x_B}{\partial \varphi} \cdot H_L \qquad \text{Eq. 4.1}$$

The combustion progress variable introduced by Vibe is defined as:

$$x_B(\varphi) = 1 - e^{a \cdot y_B^{m_V+1}} \qquad \text{Eq. 4.2}$$

where a=-6.908 corresponds to a combustion efficiency of 99.9%. y_B denotes the normalised combustion duration:

$$y_B = \frac{\varphi - \varphi_S}{\varphi_E - \varphi_S} \qquad \text{Eq. 4.3}$$

With: φ=current crank angle, φ_S=crank angle at combustion start, φ_E=crank angle at combustion end

The following parameters have been varied to match experimental data using Matlab’s lsqnonlin-function which solves non-linear least square problems:

- Ignition delay: $\varphi_{ID}=\varphi_{xB(\varphi)=5\%}-\varphi_{\text{spark timing}}$
- Burn duration: $\varphi_{BD}=\varphi_{xB(\varphi)=90\%}-\varphi_{xB(\varphi)=5\%}$
- Shape parameter m_V

Some physically based criterions have been defined to constrain the possible parameter ranges:

- The crank angle where 50% of the fuel mass is burned must agree
- Because the experimental data could not been matched very well in the late combustion period the shape of the cumulative burn rates should agree until the combustion progress reaches 70%.

Finally, the overall Vibe parameter conversion can be described by normalising the dependencies with a known reference state. The model can be defined as follows:

$$\begin{aligned} \frac{\varphi_{ID}}{\varphi_{IDO}} &= f_{RG} \cdot f_{ST} \cdot f_{rpm} \cdot f_{bmep} \\ \frac{\varphi_{BD}}{\varphi_{BDO}} &= g_{RG} \cdot g_{ST} \cdot g_{rpm} \cdot g_{bmep} \\ \frac{m_V}{m_{VO}} &= h_{RG} \cdot h_{ST} \cdot h_{rpm} \cdot h_{bmep} \end{aligned} \qquad \text{Eq. 4.4}$$

The effects of the residual gases, the spark timing, the engine speed and the engine load represented by the brake mean effective pressure are considered as the indices in Eq. 4.4 indicate. This model formulation includes the assumption that the individual effects are independent.

Starting from a reference state - where the Vibe parameters are known - the redefined combustion parameters can be determined with this set of equations.

4.2. Phenomenological combustion model

In a phenomenological way the burn rate can be described by a propagating premixed flame front and is defined by the density of the unburned mixture ρ_U, the air to fuel ratio $\lambda \cdot AF_{ST}$ - with the stoichiometric air to fuel ratio AF_{ST} -, the turbulent flame speed S_T, the turbulent flame front area A_T, the expansion factor Ex and the lower heating value H_L:

$$\frac{\partial Q_B}{\partial t} = \frac{\partial m_F}{\partial t} \cdot H_L = \frac{\dot{m}_U}{1 + \lambda \cdot AF_{ST}} \cdot H_L = \frac{\rho_U}{1 + \lambda \cdot AF_{ST}} \cdot S_T \cdot A_T \cdot Ex \cdot H_L \qquad \text{Eq. 4.5}$$

It can be seen from Eq. 4.5 that the turbulent flame speed and the turbulent flame front area have to be modelled in this formulation. In this study, experimentally determined burn rate curves are assumed to act as input parameters. This provides to define a flame front area by reversing Eq. 4.5:

$$A_T = \frac{\frac{\partial Q_B}{\partial t} \cdot \left(1 + \lambda \cdot AF_{ST}\right)}{\rho_U \cdot s_T \cdot H_L \cdot Ex} \qquad \text{Eq. 4.6}$$

The density ρ_U was taken from the backward calculation and Gülder's [6] approach for the turbulent flame speed was used:

$$\frac{s_T}{s_L} = 1 + A \cdot \left(\frac{u'}{s_L} \right)^n \cdot \mathrm{Re}_T{}^{0.25} \qquad \text{Eq. 4.7}$$

The turbulent Reynolds number is defined in Eq. 4.8. The viscosity of the unburned mixture was calculated according to Sutherland's formula:

$$\mathrm{Re}_T = \frac{u' \cdot l_i}{\nu} \text{ and } \nu = K_{visc} \frac{\sqrt{T_U}}{\rho_U} \qquad \text{Eq. 4.8}$$

The turbulence intensity u' was calculated from a one equation energy balance for the turbulent kinetic energy, where the turbulence production due to compression k_{comp}, the dissipation k_{diss}, the turbulence production due to the squish flow k_{sq} and the intake flow k_{in} are considered.

$$\frac{\partial k}{\partial t} = \frac{\partial k_{comp}}{\partial t} - \frac{\partial k_{diss}}{\partial t} + \frac{\partial k_{sq}}{\partial t} + \frac{\partial k_{in}}{\partial t} \qquad \text{Eq. 4.9}$$

For this application isotropic homogenous turbulence is assumed. Therefore, the turbulence intensity can be expressed as

$$k = \frac{1}{2} \cdot \left(u'_x{}^2 + u'_y{}^2 + u'_z{}^2 \right) = \frac{3}{2} u'^2 \quad \rightarrow \quad u' = \sqrt{\frac{2}{3} k} \qquad \text{Eq. 4.10}$$

Due to the expansion of the burnt gas the flame front propagates with a higher speed then the turbulent burning speed s_T. This is taken into account by the expansion factor Ex [7]:

$$Ex = \frac{\rho_U / \rho_B}{\left(\rho_U / \rho_B - 1 \right) \cdot x_B + 1} \qquad \text{Eq. 4.11}$$

Where ρ_B denotes the density of the burnt mixture and x_B is the combustion progress variable.

4.3. The Weller flame area model

The Weller model is a flame area model where a wrinkling factor Ξ defines the flame surface

$$\Xi = \frac{\sum}{\sum_l} \qquad \text{Eq. 4.12}$$

where $\sum$ and $\sum_l$ are the volumetric average turbulent flame area and laminar flame area, respectively.

In StarCD the equilibrium version of the Weller flame propagation is implemented. This means that the transport equation for the wrinkling factor is simplified to it's equilibrium formulation with a wrinkling generation factor G and a removal rate coefficient R:

$$R = \frac{G}{\Xi_{eq}} \qquad \text{Eq. 4.13}$$

Under these circumstances the equilibrium value Ξ_{eq} is equal to the turbulent to laminar flame speed ratio which is described with Damköhler's correlation:

$$\Xi_{eq} = \frac{S_T}{S_L} \text{ and } \frac{S_T}{S_L} = 1 + A \cdot \frac{u'}{S_L} \qquad \text{Eq. 4.14}$$

The parameter A is a model coefficient and u' is the turbulence intensity. Keck and Methgalchi's approach for the laminar flame speed, the unstrained laminar flame speed, is used, where the coefficients are adjusted depending on the equivalence ratio of the fuel:

$$S_L = S_{L0} \cdot \left(\frac{T_U}{T_0}\right)^{\alpha} \cdot \left(\frac{p}{p_0}\right)^{\beta} \qquad \text{Eq. 4.15}$$

where p is the pressure and T the temperature, the subscripts 0 and U denote unburned and reference gas properties, respectively.

To take into account the laminar flame behaviour during the early stages of flame propagation Ξ is modelled by a time delay function:

$$\Xi = 1 + \left(\Xi_{eq} - 1\right) \cdot \left(1 - e^{\frac{-(t - t_{SP})}{\tau_d \cdot \tau_\eta}}\right) \qquad \text{Eq. 4.16}$$

t_{sp} is the spark timing, $\tau_\eta = \sqrt{\nu / \varepsilon}$ is the Kolmogorov time scale and t_d is a time delay coefficient.

The mean reaction rate for the regress variable b, which is the normalised fuel mass fraction, is

$$\omega_{We} = -\rho_U \cdot Y_u \cdot S_L \cdot \Xi \cdot |\nabla b| \qquad \text{Eq. 4.17}$$

Y_u is the mass fraction of the unburned mixture and for the regress variable b - which is 1 in the unburned and 0 in the burnt gas - a transport equation is defined.

In this study the parameters t_d and A have been varied to match experimental data.

5. Results

5.1. Empirical combustion model

To test the empirical model 18 operating points have been chosen where the first nine points are without EGR and the second nine points are with EGR. From the experimentally determined burn rates the 5% burning point, the 50% burning point and the burn duration defined as 5% to 90% have been compared. Furthermore, from Eq. 4.4 it can be seen, that the results may depend on the reference state whereas this effect was investigated by testing three operating points as reference.

Before the results will be discussed it should be mentioned that the determination of the EGR rate by measuring the CO_2 concentration in the intake manifold was quite uncertain for this small engine. When the exhaust gas analyser was turned on the throttle angle had to be adjusted to keep the brake mean effective pressure due to the analyser to engine mass flow ratio. This effect could be observed especially for low load operating conditions.

Figure 1 shows the comparison between experiment and calculation for the 5% burning point. As mentioned before the results depend on the chosen reference point. The denotation in the legend consists of two numbers. The first indicates the rpm and the second the brake mean effective pressure in bar. For all these calculations the trends agree very well, whereas the variations and the differences increase for the operating points with EGR.

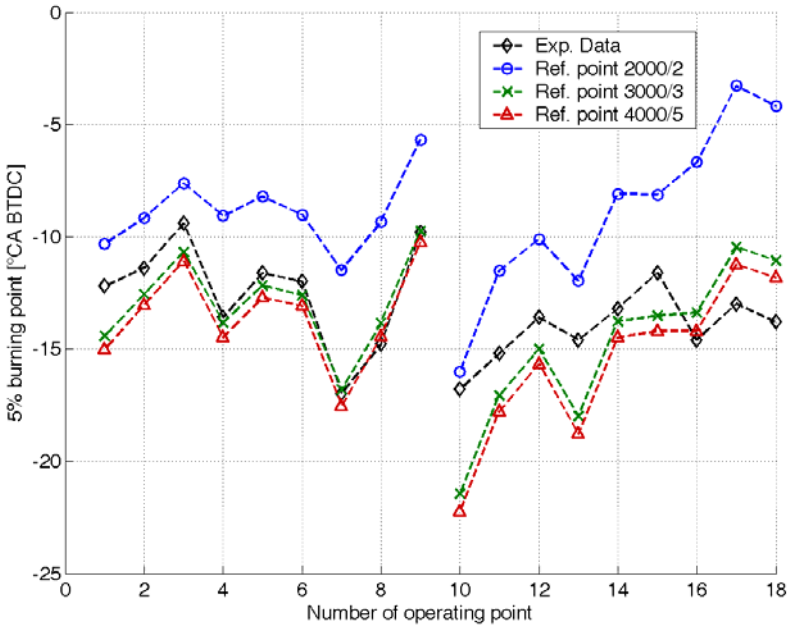

Figure 1: Experimentally determined and calculated 5% burning point

Figure 2 shows the results for the burn duration where the trends again agree quite well and the variations increase when EGR is turned on.

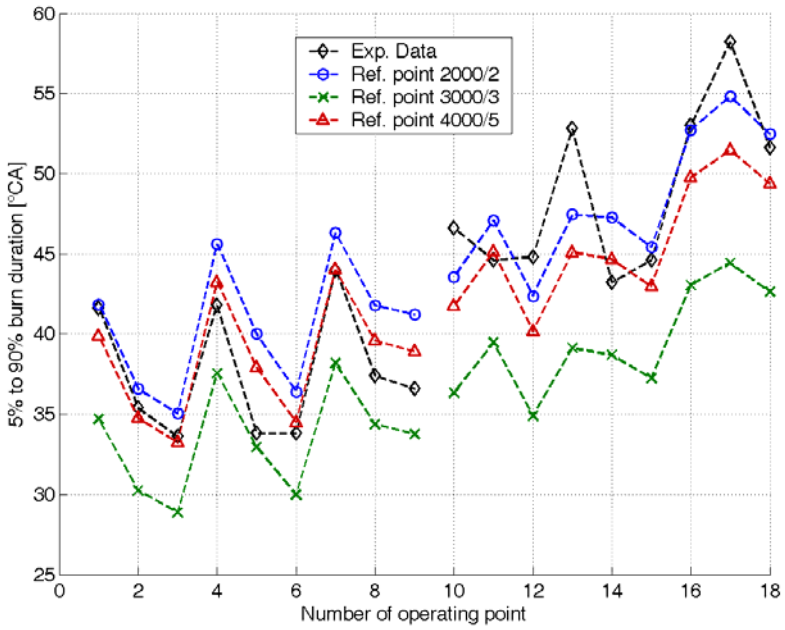

Figure 2: Experimentally determined and calculated burn duration

A similar behaviour was found for the 50% burning point. It has to be considered that these differences are a consequence of the variations of the 5% burning point and the variations of the burn duration. Nevertheless, the trends agree quite well, where most of the points are within a difference of 6 crank angles.

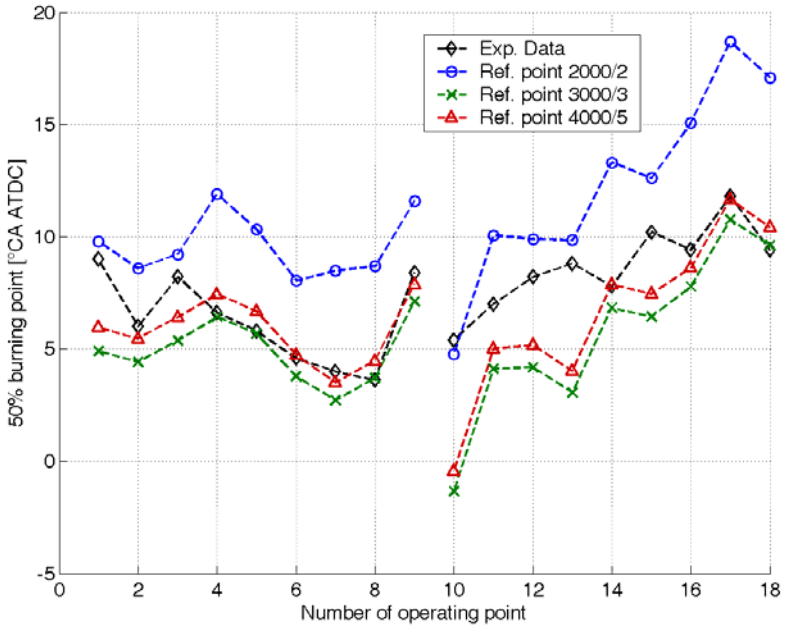

Figure 3: Experimentally determined and calculated 50% burning point

A possible reason for the reference point sensitivity can be found if the dependencies on the engine parameters are examined. The following picture shows the experimentally determined burn durations as a function of the engine speed. Furthermore, the resulting burn durations are plotted when the three reference points are applied:

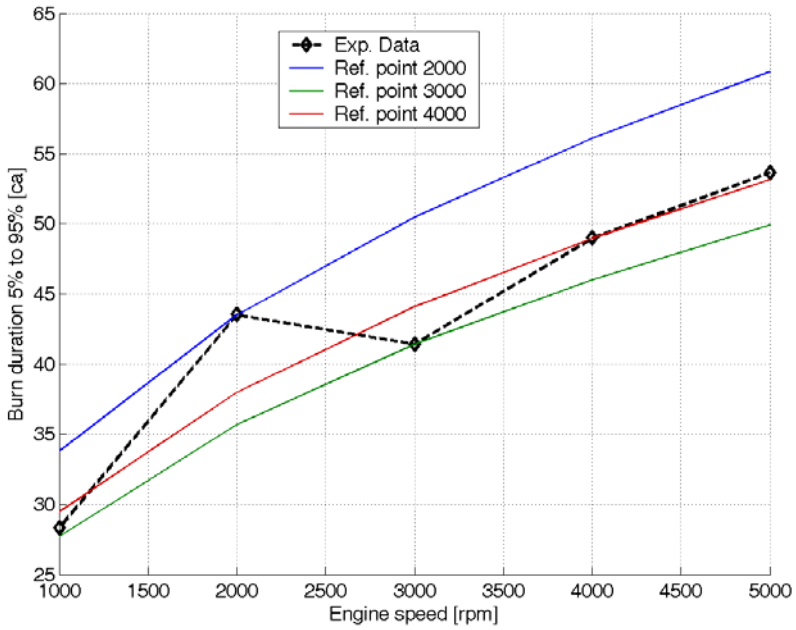

Figure 4: Burn duration as a function of engine speed (g_{rpm})

If for example an operating point with n=2000rpm is chosen as reference point, the burn duration will be too long for all other engine speeds. This may be the reason for the results illustrated in Figure 2. It has to be considered that the resulting Vibe parameters are a product of different dependencies (Eq. 4.4). Similar sensitivities were found for the ignition delay.

Finally, Figure 5 compares the indicated mean effective pressure. Excluding operating point number 13 most of the investigated operating points are within an acceptable difference. For test number 13 it is assumed that the experimentally determined EGR rate is too low where the behaviour of 5% burning, of the 50% burning points, the burn duration and the air mass flow rate confirm this assumption.

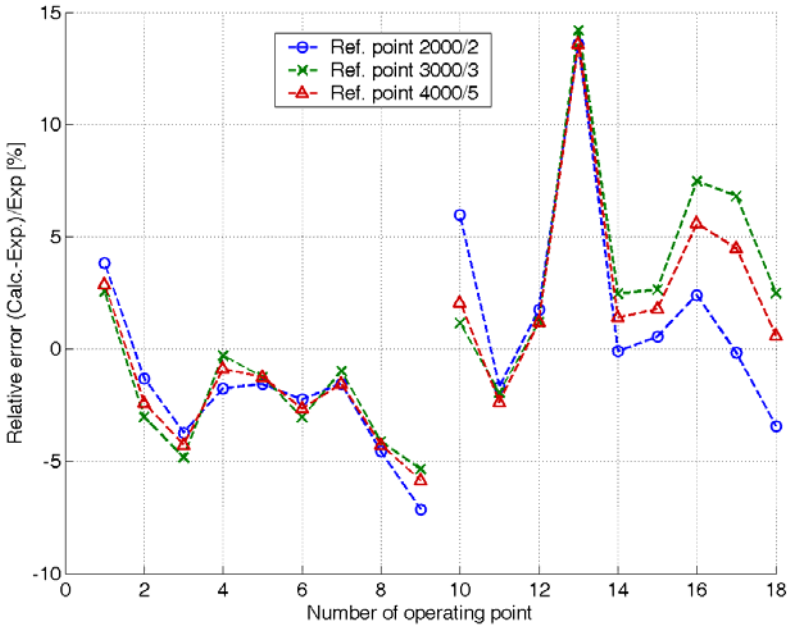

Figure 5: Relative error for the indicated brake mean effective pressure

However, applying the empirical model the effect of higher compression ratios was investigated. From the combustion chamber design it was known that a compression ratio up to ε=13.5 was practicable by changing the piston bowl. The first calculations – where the spark timing was kept constant – indicated that the compression ratio should be increased to ε=13.5. Further optimisations have been determined by varying the spark timing to see the potential.

Based on these calculations new pistons were installed to change the compression ratio of the engine to ε=13.5. Figure 6 shows the comparison for four operating points for the prediction with the empirical model and the engine test bench results based on the measurements with ε=10.7. The numbers on the x-axis indicate again the rpm and the bmep, respectively.

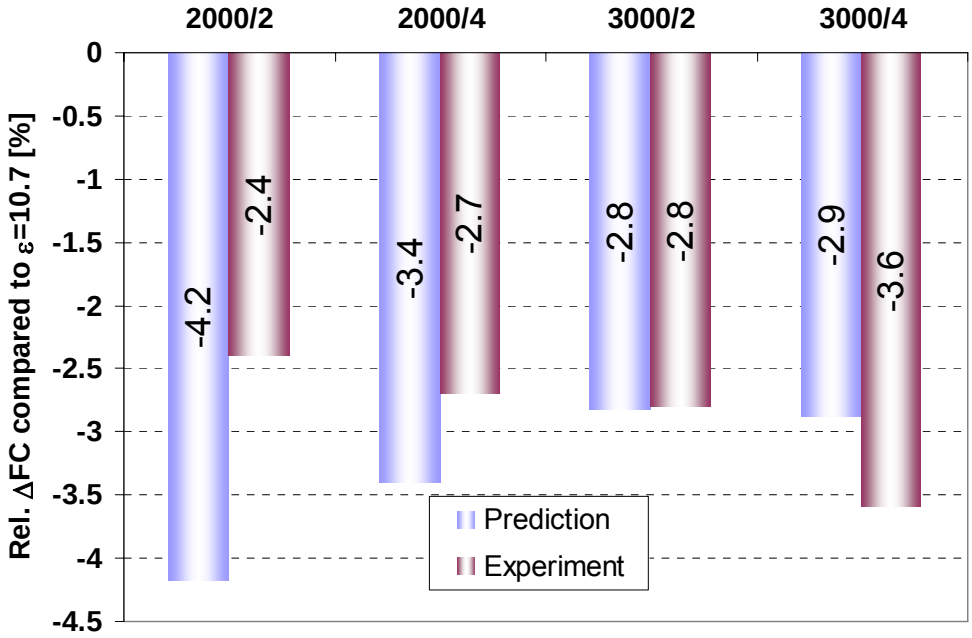

Figure 6: Prediction vs. Experiment for four operating points and ε=13.5, reference point for the simulation n=4000rpm, bmep=5bar

Due to the simple model formulation geometrical changes can not be taken into account and therefore the phenomenological model was employed to learn more about the combustion behaviour for these two combustion chamber designs.

5.2. Phenomenological combustion model

In Figure 7 the cumulative burn rate curves are compared for one operating point. The engine speed, the spark timing and the brake mean effective pressure are the same. As expected, the combustion starts earlier with higher compression ratio due to the higher temperature and pressure and burns faster in the early combustion period. From 10 crank angle after top dead centre the burning speed seems to decrease and finally the higher compression ratio case burns slower.

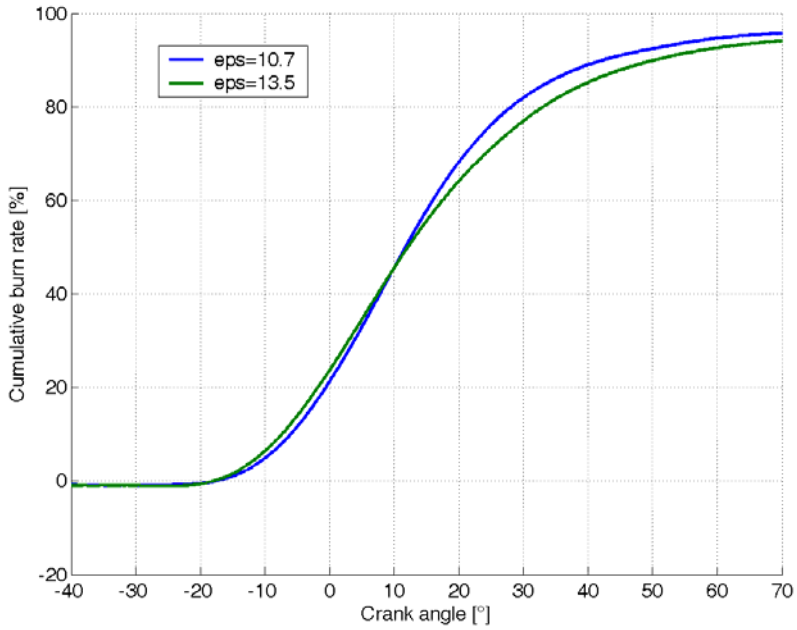

Figure 7: Cumulative burn rate curves for two combustion chamber designs, n=3000rpm, bmep=4bar, spark timing=40°BTDC

Eq. 4.6 was applied to learn more about the flame front area. Figure 8 compares these areas for both combustion chamber designs. Due to the smaller combustion chamber volume the flame front area is smaller when the compression ratio is increased. Furthermore, the curves cross at -13.5 crank angle.

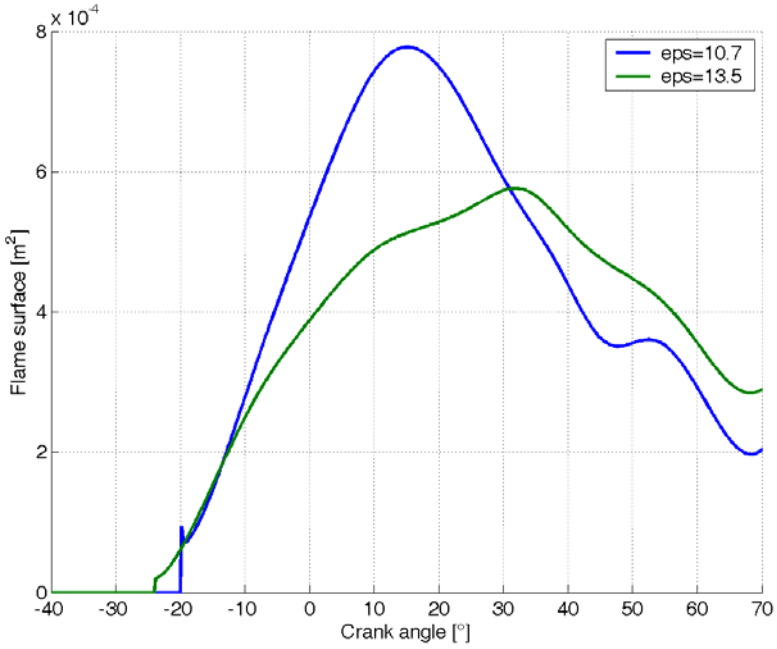

Figure 8: Flame surface for two combustion chamber designs, n=3000rpm, bmep=4bar, spark timing=40 crank angle BTDC

To determine this behaviour spherical flame propagation was assumed and a radius of a sphere was calculated. In Figure 9 a sphere with the corresponding radius is drawn into the combustion

chamber. At this time, where the flame front area curve flattens and the burn rate slows down, the flame impinges the piston.

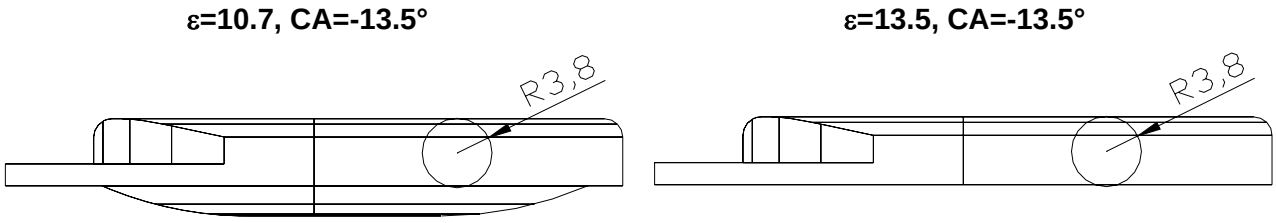

Figure 9: „Flame visualisation“ in the combustion chamber at -13.5 crank angle

This observation was very helpful to understand the combustion behaviour of the high compression ratio engine and it is encouraging that these effects could be observed by using the phenomenological combustion model. The vehicle tests from the roller test bench became comprehensible.

Based on the development illustrated in [8] a characteristic shape of the flame front area curves was found for both combustion chamber geometries.

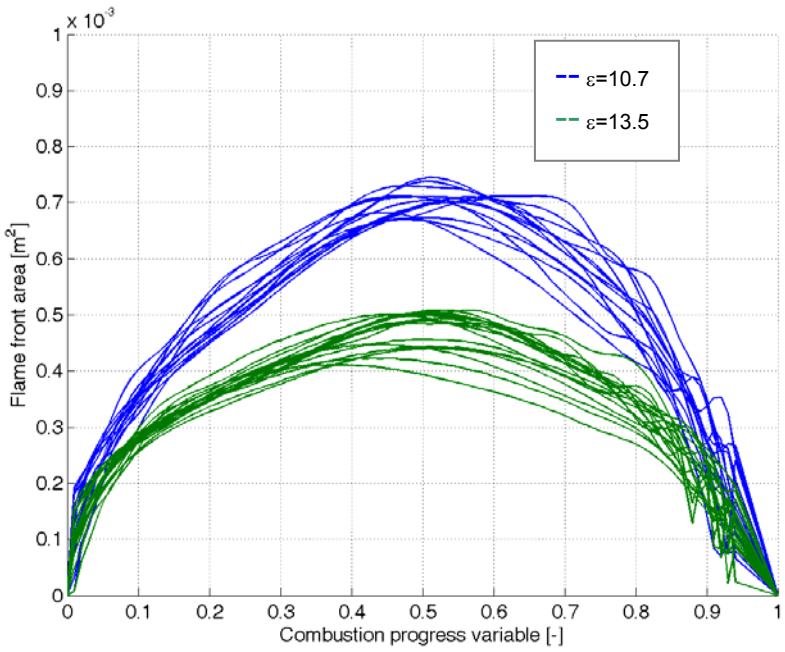

Figure 10: Characteristic flame front area curves for ε=10.7 and ε=13.5

While changes in combustion chamber geometry are not considered in the empirical model it should overestimate the advantage of an increasing compression ratio. Due to GT-Power’s friction model – the model takes into account the peak cylinder pressure and not the brake mean effective pressure as most of the friction models do - the friction of the engine increases for higher compression ratios. On the test bench this was actually not the case.

The phenomenological model will be implemented into GT-Power in the near future to have the possibility to do forward calculations and it will be compared with the empirical combustion model.

5.3. 3D calculations

Since the combustion chamber has no optical access this result has been validated using 3D calculations. The Weller flame area model described in section 4.3 was employed. The model parameters have been varied to obtain agreement between experiment and simulation. The parameters A and τ_d had to be adjusted for both combustion chamber designs and are different for the two setups. Figure 11 shows the comparison of the cumulative burn rates and Figure 12 the burn rates:

ε=10.7 **ε=13.5**

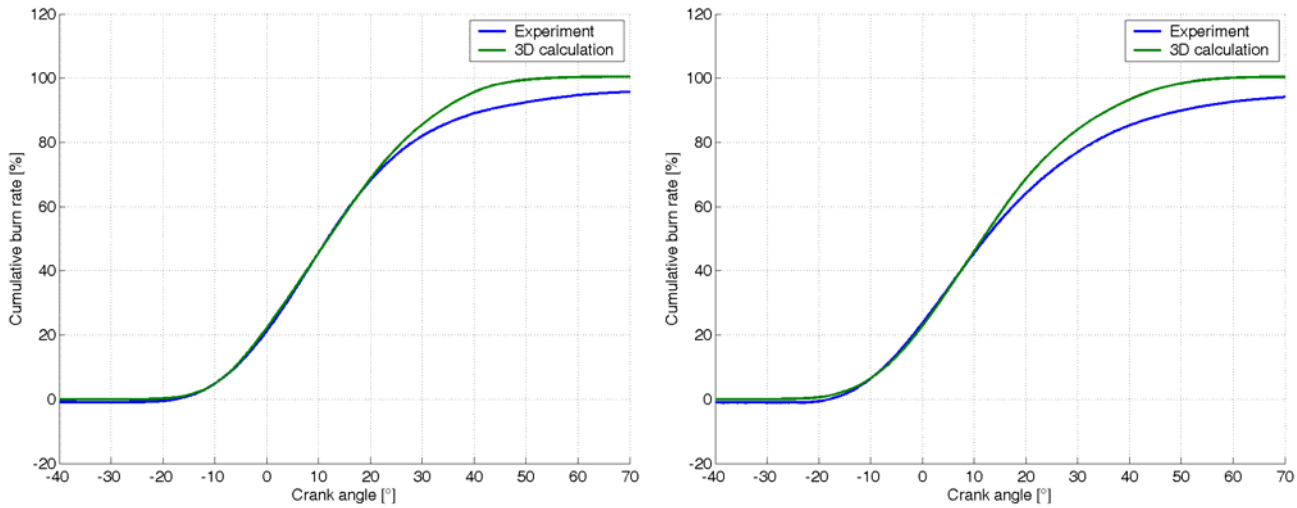

Figure 11: Cumulative burn rate curves calculated with the 3D CRFD code

ε=10.7 **ε=13.5**

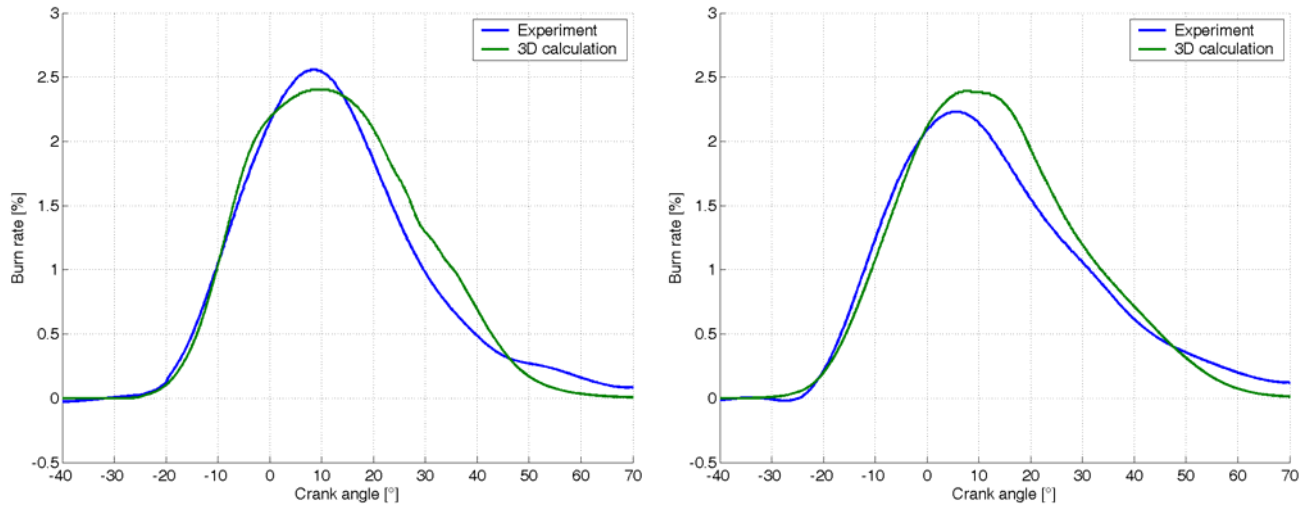

Figure 12: Burn rate curves calculated with the 3D CRFD code

The regress variable was visualised at CA=-13.5° to compare the results with the phenomenological model. In Figure 13 half of the combustion chamber can be seen. The flame impinges the piston in the ε=13.5 case at this time. The dark blue colour and the red colour indicate burnt mixture and unburned mixture, respectively. These pictures are in good agreement with the observed burning behaviour shown in Figure 7.

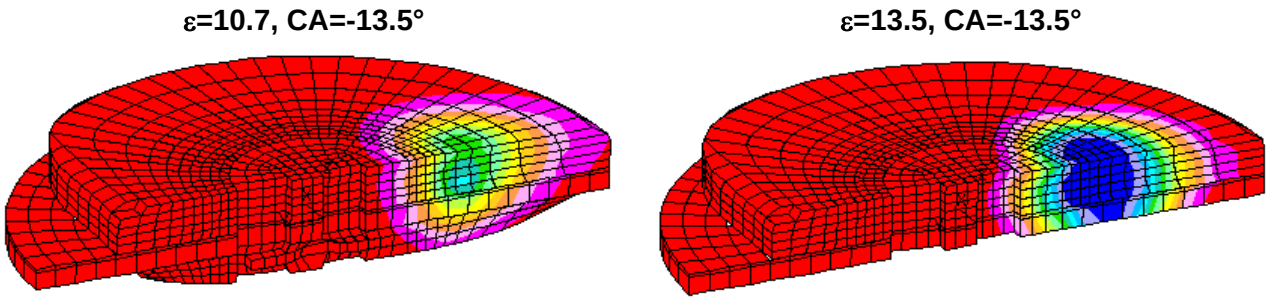

Figure 13: Combustion behaviour at -13.5 crank angle

Comparing the 3D calculation results with the observations made with the phenomenological model it can be noticed that the results seem to be meaningful.

6. Conclusions

Three types of combustion models for different applications within the development process of a new supercharged ultra-low-emission natural gas engine have been presented in this paper. An empirical combustion model was used to predict fuel consumption for different engine driving strategies where it was observed that global qualitative trends can be predicted quite well. To obtain more information about the combustion behaviour a phenomenological combustion model was used and the flame front area has been calculated and analysed. This allowed clarifying how the piston geometry affects the flame propagation. These results have finally been confirmed by detailed 3-Dimensional calculations of the in-cylinder processes.

Every class of model can be applied in a meaningful way. The application depends on the objectives of the specific stage during the research and development process.

The empirical models can be used when computational time demand is critical. On the other hand, these models can not take into account parameter changes when extrapolating trends, because they are based on limited physical insights.

The phenomenological models in contrast do consider to some degree physicochemical and geometric effects during combustion. These models have therefore the potential to be useful in understanding and predicting fluid mechanical phenomena for extended deviations from measured operating conditions. They however also need some calibration through experiments.

The 3-Dimensional calculations revealed interesting local effects of flame propagation in support of the phenomenological model. Although not free of model parameters adjustment, this class of tools can be used nowadays efficiently to interpret and understand in-depth experimental findings and partially to predict changes of parameters, which are out of reach for the other two groups of models.

The final conclusion of this work is that every class of model is tailored to specific needs of the product development process which can be significantly accelerated if a synergetic approach combining targeted experiments and different computational models is carefully selected for each specific application.

7. Acknowledgments

The authors would like to thank:

- The Swiss Federal Office of Energy SFOE, the Swiss Gas and Water Industry Association SVGW, the German technical and scientific organisation on Gas and water DVGW and the Austrian Gas and Water Industry Association ÖVGW.

- Our industrial partners: VW, Bosch, Corning, Engelhard

- Rolf Ziegler and Roland Graf at the EMPA, CH-Dübendorf

- Peter Eberli, Gerhard Egli, Marcel Décosterd and Peter Obrecht at the Aerothermochemistry and Combustion Systems Laboratory (LAV), ETH Zurich

8. References

[1] 8. Berichterstattung im Rahmen der Energieverordnung über die Absenkung des spezifischen Treibstoff-Normverbrauchs von Personenwagen 2003, Auto-Schweiz, 2003

[2] Communication from the commission (...) on alternative fuels for road transportation and on a set of measures to promote the use of biofuels, COM(2001) 547 final, 2001

[3] Monitoring of ACEA's Commitment of CO2 Emission Reductions from Passenger Cars, Final Report, September 2003

[4] **Bach, C. et al.:** *Clean Engine Vehicle - A Natural Gas Driven Euro-4/SULEV with 30% Reduced CO2-Emissions*, SAE Technical paper 2004-01-0645, 2004

[5] **Csallner, P.:** *Eine Methode zur Vorausberechnung der Änderung des Brennverlaufes von Ottomotoren bei geänderten Betriebsbedingungen*, Dissertation TU München, 1981

[6] **Gülder, Ö. L.**: *Turbulent Premixed Flame Propagation Models for Different Combustion Regimes*, Twenty-Third Symposium (International) on Combustion, The Combustion Institute, p. 743-750, 1990

[7] **Heywood, J. B.:** *Internal Combustion Engine Fundamentals*, McGraw-Hill International Editions, 1988

[8] **Koch, Th.:** *Numerischer Beitrag zur Charakterisierung und Vorausberechnung der Gemischbildung und Verbrennung in einem direkteingespritzten, strahlgeführten Ottomotor*, Dissertation ETH Zürich, 2002

[9] **Witt, A.:** *Analyse der thermodynamischen Verluste eines Ottomotors unter den Randbedingungen variabler Steuerzeiten*, Dissertation TU Graz, 1999

[10] **Zeilinger, K., Zitzler, G.:** *Vorausberechnung der Brennverläufe von Gasmotoren*, MTZ 64 (12), p. 1080-1089, 2003